Regulation of in vitro Calcium Phosphate Mineralization by Combinatorially Selected Hydroxyapatite-Binding Peptides

ARTICLE *in* BIOMACROMOLECULES · APRIL 2008

Impact Factor: 5.75 · DOI: 10.1021/bm701037x · Source: PubMed

6 AUTHORS, INCLUDING:

Mustafa Gungormus
Yıldırım Beyazıt Üniversitesi
25 PUBLICATIONS **351** CITATIONS
SEE PROFILE

Candan Tamerler
University of Kansas
132 PUBLICATIONS **3,427** CITATIONS
SEE PROFILE

Mehmet Sarikaya
University of Washington Seattle
139 PUBLICATIONS **4,805** CITATIONS
SEE PROFILE

Regulation of in vitro Calcium Phosphate Mineralization by Combinatorially Selected Hydroxyapatite-Binding Peptides

Mustafa Gungormus,[†] Hanson Fong,[†] Il Won Kim,[‡] John Spencer Evans,[‡] Candan Tamerler,[*,§] and Mehmet Sarikaya[*,†]

University of Washington, Seattle, Washington, New York University, New York City, New York, and Istanbul Technical University, Istanbul, Turkey

Received September 17, 2007; Revised Manuscript Received November 13, 2007

We report selection and characterization of hydroxyapatite-binding heptapeptides from a peptide−phage library and demonstrate the effects of two peptides, with different binding affinities and structural properties, on the mineralization of calcium phosphate mineral. In vitro mineralization studies carried out using one strong- and one weak-binding peptide, HABP1 and HABP2, respectively, revealed that the former exhibited a drastic outcome on mineralization kinetics and particle morphology. Strong-binding peptide yielded significantly larger crystals, as observed by electron microscopy, in comparison to those formed in the presence of a weak-binding peptide or in the negative control. Molecular structural studies carried out by circular dichoroism revealed that HABP1 and HABP2 differed in their secondary structure and conformational stability. The results indicate that sequence, structure, and molecular stability strongly influence the mineralization activity of these peptides. The implication of the research is that the combinatorially selected short-sequence peptides may be used in the restoration or regeneration of hard tissues through their control over of the formation of calcium phosphate biominerals.

Introduction

Inorganic materials synthesized by biological organisms (biomineralization) often possess unique and optimal morphological and structural properties and serve as ideal models in designing and engineering of functional biomimetic materials. One key aspect of biomineralization is the participation of biomacromolecules such as glycoproteins and phosphoproteins.[1] That proteins influence nucleation, crystallography, polymorphism, and morphology of biogenic inorganics[1,2] has led to development of approaches to utilize them in controlled in vitro mineralization processes. The traditional approach involves using proteins that are extracted and purified from hard tissues in in vitro mineralization experiments.[3,4] Although there are exciting examples, the biomineralization using isolated proteins is limited mainly because of the difficulties involved in the extraction and purification of these proteins from the biological systems and the characterization of their functions. Another approach in using proteins in materials is de novo design via the predictive methods.[5] Usually there may be a large number of proteins with various temporal and spatial distribution involved in a given biological mineralization process. It is impractical, for the time being, to expect all proteins to be extracted and purified or their sequences to be available in the existing protein databases. Therefore, practical biomineralization toward tissue regeneration using proteins extracted from hard tissues or those de novo designed remains elusive.

There is a third and, possibly, a more practical approach. The utility of combinatorially selected peptides through viral- or bacterial-displayed peptide libraries has recently proven to be an effective technique for generating polypeptide sequences that have specific affinities to a variety of inorganic surfaces.[6,7] In this approach, a pool of random amino acid sequences, displayed on the surface of a host organism, are exposed to a target inorganic substrate and the mutant organisms displaying specific binding sequences are selected.[8] Several groups have applied this approach successfully to identify inorganic binding peptides and utilized them for various applications including making templated conjugates, producing protein-encapsulated particles and synthesis of nanoparticles and minerals.[7] Given that these genetically engineered peptides for inorganics (GEPI)[6] recognize and bind to solid materials, there may also be an inherent capability within the sequences to influence morphology of these minerals as well, an opportunity which has not yet been fully explored in great detail so far.

Here, we report selection of HA-binding peptides using a combinatorial expression technique to generate a set of sequences that could offer a route for controlling calcium phosphate-based biomineral formation within a biomedical context. Specifically, this study involves a successful screening of a cysteine-constrained M13 bacteriophage heptapeptide library against hydroxyapatite (HA) powder. Using the library, we selected more than 50 sequences and two were identified for further investigation, one that exhibited the highest binding affinity (HABP1), and the other, a much lower binding affinity (HABP2) to HA, for subsequent calcium phosphate formation and physicochemical characterization studies. Here, we were interested in learning if HA-binding polypeptides sequences could also regulate calcium phosphate formation in vitro and likewise determine the contributions of primary sequence and secondary structural properties that are associated with HA affinity as well as calcium phosphate formation capability. As described here, we found that both HABP1 and HABP2 did affect calcium phosphate formation, with the former exhibiting a higher inhibitory activity over the latter. Finally, we attempt to explain the observed significant differences of morphogenesis

* Author to whom correspondence should be addressed. E-mail: sarikaya@u.washington.edu (M.S.); tamerler@itu.edu.tr (C.T.).
[†] University of Washington.
[‡] New York University.
[§] Istanbul Technical University.

10.1021/bm701037x CCC: $40.75
Published on Web 02/14/2008

of the inorganic particles formed based on the molecular structural features of the peptides, determined by circular dichroism.

Materials and Methods

Selection of Hydroxyapatite-Binding Peptides. Ph.D.-C7C Phage Display Peptide Library Kit was purchased form New England BioLabs Inc. This kit is based on a combinatorial library of random peptide 7-mers fused to the minor coat protein (pIII) of M13 phage. The randomized sequences are flanked by a pair of cysteine (Cys) residues. Under nonreducing conditions, the cysteines form a disulfide cross-link, resulting in display of constrained peptides. Synthetic hydroxyapatite powder was used as target substrate. (Ivan Transevica Institute, Department of Materials Science, Ukraine). Prior to exposing to the peptide−phage library, the powder surface was cleaned by, first, ultrasonicating in a methanol/acetone mixture and then repeating the ultrasonication in isopropanol. Cleaned HA powder was then incubated with phage−peptide library overnight in a potassium phosphate/sodium carbonate (PC) buffer (pH 7.4), containing 0.1% detergent (Tween 20 and Tween 80, Merck) at room temperature with constant rotating. The detergent prevents nonspecific interactions between phage particles and facilitates individual phage particle−powder surface interaction. After incubating the HA powder substrate with the phage library, the powder was washed several times with PC buffer containing 0.1% detergent to remove the nonspecifically or weakly bound phage particles from the HA surfaces. The phages remaining on the HA surface were then eluted by 0.2 M glycine HCl (pH 2.2) solution followed by ultrasonication (see Supporting Information). Eluted phages were transferred to an early log phase *E. coli* ER2738 culture and amplified for 4 h. The amplified phages were isolated by polyethylene glycol (PEG) precipitation. In the subsequent rounds, fresh HA powder substrate was exposed to the phages obtained from the previous round to enrich the phage pool in the favor of the most strongly binding clones. After the third round, the phages obtained from each round were plated on LB-agar media containing 5-bromo-4-chloro-3-indolyl-β-D-galactopyranoside (Xgal) and isopropyl-β-D-thiogalactopyranosid (IPTG) in serial dilutions to obtain single phage plaques. Because the ER2738 strain lacks the lacZ α gene, only the cells infected by M13mp 19 bacteriophage, carrying the lacZ α gene, can produce competent β-galactosidase. Therefore, infected cells can hydrolyze X-Gal and form blue phage plaques. After growing the phages on LB-agar plates, single blue plaques containing monoclonal phage particles were picked, amplified, and the amino acid sequence of the randomized polypeptide segment was identified by DNA sequencing.

Characterization of Phage Binding to HA via Immunofluorescence Microscopy. Cleaned HA powder was incubated overnight with selected monoclonal phages at 10^{11} PFU/mL concentration in PC buffer containing 0.1% detergent at room temperature and with constant rotating. Wild type (WT) M13mp 19 bacteriophage, displaying no peptides on the pIII protein, was used as negative control. After the incubation, the powder was washed three times with the same buffer. After the washing, the phages that remained bound to the surface were labeled with mouse AntiM13 IgG (Amersham Biosciences) and Alexa Fluor 488−antimouse IgG_{2a} conjugate (Invitrogen Corporation). After the labeling, the powder suspension was transferred to a microscope slide and observed using a TE 300L microscope (Nikon, Japan). Approximate surface coverage of the phage particles was calculated using MetaMorph Imaging System version 6.2 (Photometrics UK Ltd., UK, formerly Universal Imaging Co., USA) by comparing the approximate surface area of the powder in the bright field image to the approximate phage coverage in the fluorescence image. Phage clones were grouped as strong, moderate, and weak binders according to their surface coverage.

Characterization of Phage Binding to HA via Enzyme-Linked Immunosorbent Assay (ELISA). Cleaned HA powder was incubated overnight with selected monoclonal phages at 10^{11} PFU/ml concentration in PBS buffer containing 2% BSA at room temperature with constant rotating. Wild type M13mp 19 bacteriophage, displaying no peptides on the p(III) protein, was used as negative control. The powder was washed three times with PBS buffer containing 0.05% detergent. After the washing, the bound phages on the surface were labeled with horseradish peroxidase (HRP)−AntiM13 IgG conjugates (Amersham Biosciences) in PBS buffer containing 2% BSA for 30 min with constant rotating and washed four times with PBS buffer. The reaction ready HRP substrate one-step TMP-ELISA (Pierce) was added into the solution. Reaction was stopped after 2 min by adding 1 M H_2SO_4. The optical density (OD) of the reaction solution was measured at 450 nm wavelength using a microplate reader (Tecan Trading AG, Switzerland).

Subsequently, from these immunofluorescence and ELISA studies, a high affinity sequence, CMLPHHGAC (HABP1), and a low affinity sequence, CNPGFAQAC (HABP2), were synthesized using standard *Fmoc* solid-phase peptide synthesis techniques and purified using C-18 reverse-phase liquid chromatography (RPLC) to a level >95% (United Biochemical Research). Both of the chemically sequenced peptides used here were Cys−Cys constrained to mimic the native peptides with random sequences in the library that were Cys−Cys constrained and displayed on the pIII coat protein of M13 bacteriophage.

In Vitro Biomineralization Studies with Constrained HABP1 and HABP2 Synthetic Peptides. To investigate the effect of HABP1 and HABP2 on in vitro calcium phosphate nucleation, an alkaline phosphatase (AP) based mineralization system was used. Here the objective was to mimic biological mineral formation, where the phosphate release is controlled by the enzyme AP. Prior to the mineralization experiments, the activity of AP was measured in the presence of no peptide, and of synthetic HABP1 and HABP2 peptides, to assess the effects of either peptide on the enzyme activity. β-Glycerophosphate (β-GP, 14.4 mM) solutions containing no peptide and 0.4 mM HABP1 and HABP2 peptides were prepared in 25 mM Tris-HCl buffer (pH 7.4). Reaction was started by adding 1.4×10^{-6} g/mL bacterial AP (Fermentas) to the solutions. The reactions were carried on at 37 °C, and samples were collected at times 0.25, 0.5, 1, 1.5, 2, 3, and 24 h. The released phosphate concentration in each solution was measured using PiPer Phosphate Assay Kit (Invitrogen Co.).

For mineralization experiments, a mineralization solution containing 24 mM Ca^{2+} and 14.4 mM β-GP was prepared in 25 mM Tris-HCl buffer (pH 7.4) in a standard 96 well plate as triplicates. Bacterial AP (Fermentas), 1.4×10^{-6} g/mL, was added to the solutions to start the mineralization. Because the mineralization solution did not contain inorganic phosphate to initiate the mineralization process, hydrolysis of β-GP by AP and release of one inorganic phosphate group facilitated the mineralization. This enabled a detailed time-wise study of the mineralization. Mineralization solutions containing 0.07 mM and 0.4 mM peptides were prepared by dissolving the lyophilized HABP peptides in 250 μL mineralization solution in a standard 96 well plate. A mineralization medium containing no peptide was prepared as the negative control reaction. Mineralization reactions were commenced by adding bacterial AP to the mineralization medium at a final concentration of 1.4×10^{-6} g/mL. Subsequent mineral formation was monitored by continuous measuring of absorbance increase at 820 nm wavelength using a Tecan Safire microplate reader (Tecan Trading AG, Switzerland) and periodic assays of calcium and phosphate ions throughout the reaction. All mineralization reactions were carried out at 37 °C.

For periodic assays of calcium and phosphate, 10 μL of the reaction solution was collected at 0.25, 0.5, 1, 1.5, 2, 3, 4, 5, 6, 24, 48, 64, and 96 h. AP was inactivated after sample collection by immediate heating up to 90 °C for 10 min and then cooling down to –20 °C to prevent the phosphate release to proceed after the sample collection. The mineralized phase was separated by centrifuging at 9500 *g* for 10 min. Supernatant was removed and transferred to a fresh tube, and the precipitated mineral phase was washed three times with DI water to

remove excess salts. Then the mineral phase was dissolved by adding 10% nitric acid. The calcium and phosphate concentrations were determined using QuantiChrome Calcium Assay Kit (Bioassays) and PiPer Phosphate Assay Kit (Invitrogen Co.). The sample solutions were neutralized by 0.1 M Tris buffer (pH 9.1) prior to the measurements.

Electron Microscopy Analysis. Samples were collected for SEM and TEM analyses for time points of 0.5, 1.5, 2.5, 28, and 96 h for each reaction condition. Sample collection involved taking a 10 μL aliquot from the reaction solution and placed onto a carbon coated TEM grid. After 1 min, liquid on the TEM grid was carefully wicked away immediately followed by vacuum-drying for 5 min. The dried grid was stored in a desiccated container for SEM and TEM analyses. SEM characterization was performed at 10 kV using a JSM 7000F (JEOL) SEM in secondary electron imaging mode. TEM imaging and diffraction were performed using an EMS 420T (FEI, Inc., USA; formerly Philips, The Netherlands) TEM at 120 kV.

Circular Dichroism Experiments. Lyophilized HABP1 and HABP2 synthetic peptides were individually dissolved in distilled–deionized water to create stock solutions. Each stock solution was diluted to 50, 30, 20, 15, 12, 9, and 6 μM for CD spectrometry measurements in 100 μM Tris-HCl (pH 7.5). On the basis of the concentration variation studies, the optimal concentration was chosen as 30 μM, and this concentration was utilized for further 2,2,2-trifluoroethanol (TFE) (Acros Chemicals, 99.8%) titration studies (10, 30, 50, 70, and 90% by volume). All CD spectra were obtained at 25 °C with an AVIV 60 CD spectrometer (Aviv Associates) running 60DS software version 4.1t. The CD spectrometer was previously calibrated with D-10-camphor-sulfonic acid. Wavelength scans were conducted from 185 to 260 nm with appropriate buffer and solvent background subtraction. For each spectra, three scans were averaged using 1 nm bandwidth and a scanning rate of 0.5 nm/s. Mean residue ellipticity $[\theta_M]$ is expressed in deg·cm^2·dmol^{-1}.

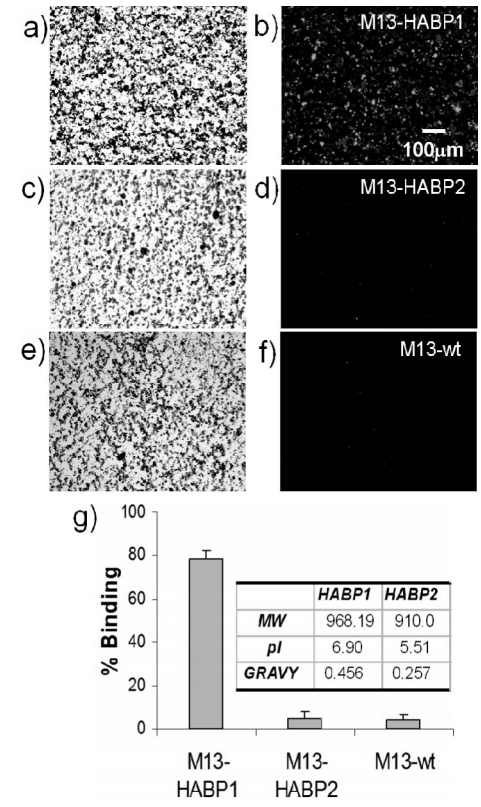

Figure 1. Bright field (a,c,e) and corresponding immunofluorescent (b,d,f) images of M13 bacteriophage displaying HABP1, HABP2, and wild type (WT) M13, respectively, on HA powder samples. The binding affinities determined by ELISA (g). Inset: physicochemical properties of the selected strong- and weak-binding sequences with constraint loop architectures.

Results and Discussion

The phage−peptide library used in this study was based on Cys−Cys constrained random heptapeptides fused to the minor coat protein (pIII) of the M13mp 19 bacteriophage. After three biopanning rounds, 56 clones were selected (18 from first round, 19 each from second and third rounds) and characterized in terms of their physicochemical properties and binding affinity to HA. On the basis of immunofluorescence microscopy assays, out of 56 clones, 12 were characterized as strong binders with a surface coverage higher than 40%, 28 were moderate binders with a coverage between 35% and 10%, and 16 were weak binders with a coverage lower than 7%. In addition, ELISA was used to confirm these results and the data obtained from both techniques were consistent. Statistical analysis of the binders after binding characterization revealed that 67% of the strong binders were selected in the third round of panning; likewise, 69% of the weak binders were selected in the first round of panning (see Supporting Information). These results showed that selection of strong-binding clones was favored in the additional panning rounds.

The strongest binding clone (CMLPHHGAC, 75 + 5% binding) and a weak-binding clone (CNPGFAQAC, 3 + 2% binding) were chosen for subsequent solid-phase peptide synthesis and mineralization experiments (Figure 1a−g). We will subsequently refer to these individual synthetic peptides as HABP1 (strong binder) and HABP2 (weak binder), respectively. One reason for choosing these two sequences was that both share similar physicochemical properties yet each exhibit vastly different HA-binding affinities. Molecular weights of the peptides are 968.1 for HABP1 and 910.0 for HABP2. The *pI* values of HABP1 and HABP2 were calculated as 6.90 and 5.51, respectively (using the ExPASy prot-param tool of the Swiss Institute of Bioinformatics). The HABP1 has charged side chains (His) within the conditions of in vitro mineralization experiments of pH 7.4. Also, according to the calculated grand average of hydropathicity (GRAVY) values, both peptides are water soluble and stable in solution (Figure 1g).

Effects of HA-Binding Sequences on Calcium Phosphate Mineralization. An AP-mediated mineralization system was used to demonstrate the effects of the selected peptides on mineral precipitation. This system involves enzymatic hydrolysis of an organic phosphate compound, namely β-GP, by AP, which enables slow release of phosphate ions. In previous studies using this mineralization platform, both amorphous (ACP) and crystalline (OCP, HA) phases of calcium phosphate minerals have been reported to form in vitro.[9] The advantage of this assay in our case is that it facilitates controlled kinetics and time-wise analyses of morphogenesis of the calcium phosphate mineralization in the presence and absence of the peptides. An important issue in this process, however, is that the enzymatic activity of AP may be affected by the presence of peptides. To assess this potential phenomenon, prior to the mineralization experiments, the activity of AP was measured in the presence of the either HABP1 or HABP2 and in the absence of any peptide, i.e., the negative control. In all cases, a fast phosphate release was observed during the first 30 min, with a reaction constant of 0.014/min, followed by a slower release, with a reaction constant of 0.0017/min. We conclude, therefore, that any influence in the kinetics of mineralization or the change in morphology of crystals is due to the effects that originate from the presence of either of the peptides in the mineralization solution.

Addition of synthetic HABP1 and HABP2 peptides to the mineralization solutions resulted in the delayed precipitation in

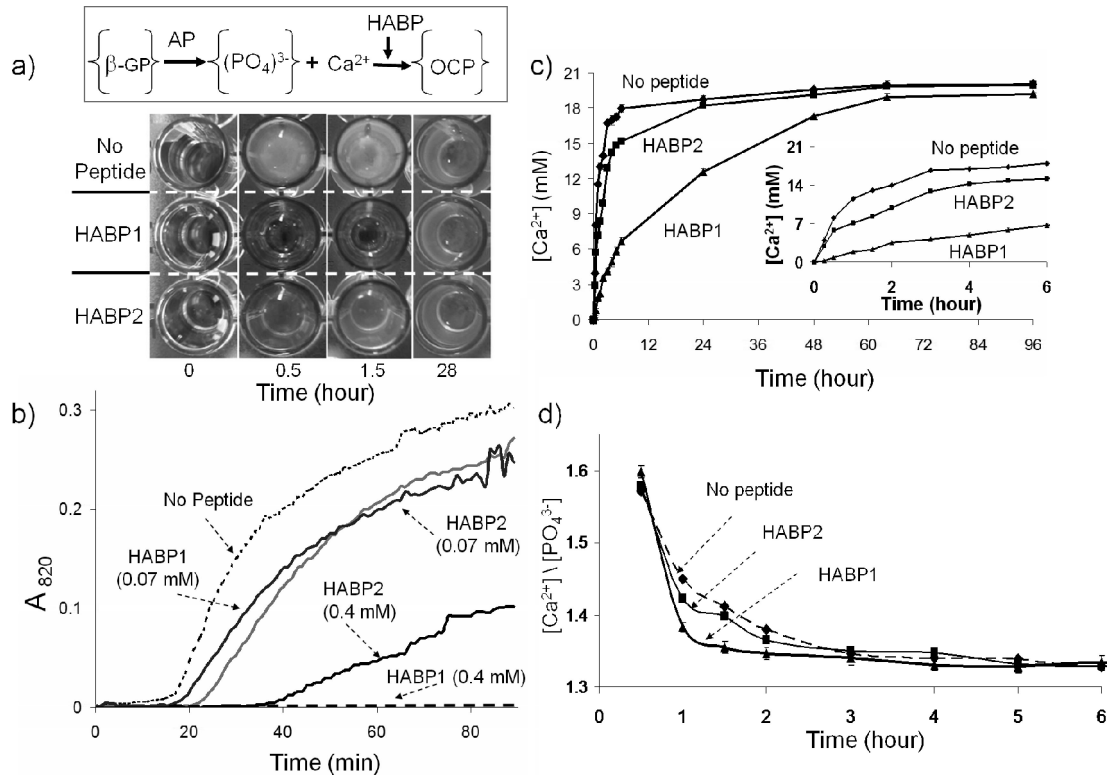

Figure 2. (a) Optical image of mineralization media in the presence of no peptide, HABP1, and HABP2 at 0, 0.5, 1.5, and 28 h. (b) Change in optical density of mineralization media at different peptide concentrations. (c) Rate of Ca^{2+} consumption in the presence of peptides; inset: the consumption rate during the first 6 h. (d) Ca/P ratio of the mineral phase at different time points.

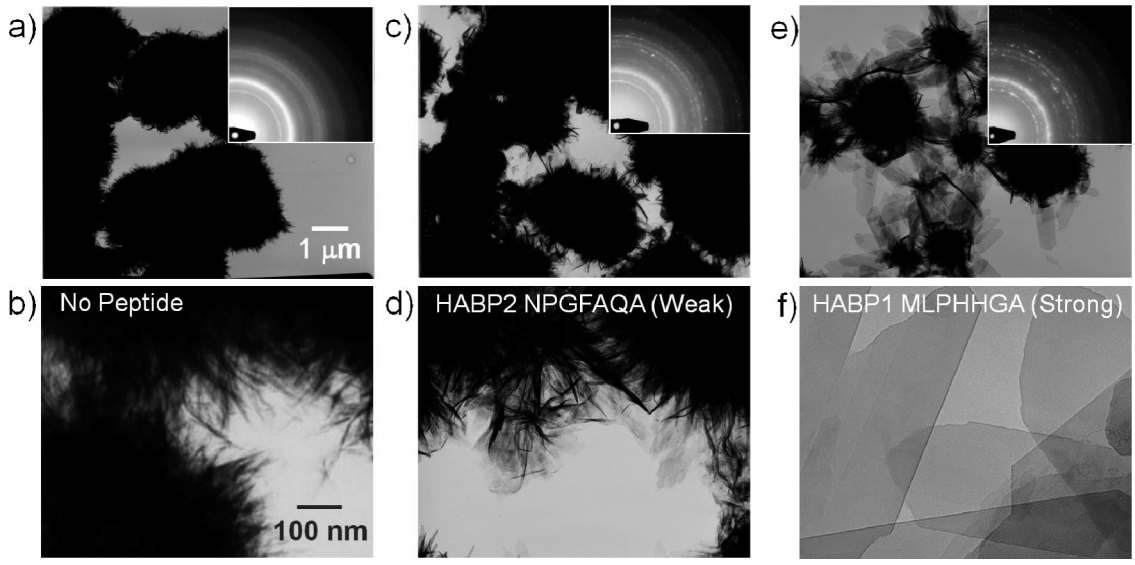

Figure 3. TEM BF images of the inorganic particles formed in the presence of: no binder (a,b), HABP2 (c,d), and HABP1 (e,f) at 96 h. Insets in (a), (c), and (e) are the corresponding selected area diffraction patterns of the minerals. The scale bar in (a) applies to (c) and (e), and that in (b) applies to (d) and (f).

a dose-dependent manner that was monitored by in situ optical density measurements (Figure 2b). The highest rate of increase in optical absorbance was observed with the negative control reaction, containing no peptide in the mineralization solution. In the presence of HABP2 and HABP1, respectively, the increase of the absorbance was reduced and the onset of the absorbance increase was delayed (Figure 2b). At 0.07 mM peptide concentration, a minor reduction was observed in the absorbance increase for both HABP1 and HABP2. However, at 0.4 mM peptide concentration, the absorbance was reduced to about one-third of the negative control reaction in 90 min with the HABP2 reaction, and a drastic reduction to almost no increase was observed with HABP1 reaction (Figure 2b). As shown in Figure 2a, optical images of mineralization solutions in the presence of 0.4 mM HABP2 and HABP1 were compared against the negative control reaction at different time points. Again, for assay periods up to 90 min, the turbidity of the reaction media was in descending order of negative control, HABP2 and HABP1, with HABP1 appearing clear. However, at 28 h, turbidity of the reaction media was similar in all three cases, indicating that sufficient mineralization had taken place.

For peptide concentrations of 0.4 mM, the reaction kinetics was further quantified by monitoring the rate of Ca^{2+} and PO_4^{3-} consumption. As shown in Figure 2c, the consumption rate of Ca^{2+} was significantly delayed in the presence of HABP1 compared to that of HABP2 and the negative control. The initial 3 h of Ca^{2+} consumption obeyed first-order reaction kinetics for all three cases, with rate constants of 0.0079/min, 0.0039/min, and 0.0012/min for no-peptide control, HABP2, and HABP1, respectively. Clearly, the rate of mineralization was reduced by more than 6-fold in the presence of HABP1, compared to the negative control. A similar trend was also observed for PO_4^{3-} consumption rate, with HABP1 reaction being significantly slower compared to those of HABP2 and negative control (see Supporting Information). Besides a decrease in the precipitation rate, an increase was observed in the conversion rate of amorphous calcium phosphate (ACP, $Ca_9(PO_4)_6$) to crystalline octacalcium phosphate (OCP, $Ca_8(HPO_4)_2(PO_4)_4 \cdot 5H_2O$) in the presence of HABP1. The values of Ca/P ratio for ACP and OCP are 1.55 and 1.33, respectively. As shown in Figure 2d, the Ca/P ratio in the control and the HABP2 reactions reached to 1.33 in about 3 h, while the same ratio was reached in approximately 1.5 h in the presence of HABP1 (Figure 2d).

Analysis of Mineral Phase Formed in the Presence of HABPs. Interestingly, the mineral phase formed in negative control and all experimental assays was OCP and not HA, as quantitatively determined by electron diffraction analysis (Figure 3) but could also be assessed from the morphology. We also have achieved formation of HA with slight modifications in our experimental conditions, such as using N_2 atmosphere or adding of F^- ions without changing any other parameters.[4h] The HABP1 and HABP2 exhibited a similar effect on the mineral morphology when the final product was HA, i.e., larger HA crystals were observed in the presence of HABP1 compared to that of HABP2 and no peptide. However, the effect on the morphology was much less pronounced when direct HA formation was induced instead of OCP. The OCP has generally been considered as one of the precursor phases in calcium phosphate biomineralization prior to subsequent transformation to a more stable HA by a hydrolysis reaction in organisms.[10] Also, the OCP has been shown to have better osteoconductive and osteoinductive properties because it is a more resorbable phase than HA.[10de] Our results, therefore, may have additional significant implications in that the proteins known to bind to HA in biological hard tissues (e.g., BMPs, bone morphogenetic proteins, in bone and amelogenin in enamel) influence the HA crystal size and shape via more complex mechanism(s) than by simply binding to HA. These proteins may affect the eventual HA morphology indirectly by controlling the morphology of the intermediate phases prior to the transition to a more stable HA.

TEM observations revealed that, in the presence of HABP1, the dimensions of the OCP crystals were significantly larger than those formed in the presence of HABP2 or in the negative control (Figure 3). In the absence of any peptide, the final morphology of the particles appeared as platelike crystals that collectively formed a characteristic spherulite microstructure (Figure 3a,b). This morphology, but with slightly larger crystal widths (20–30 nm, and less than a μm), was also observed in the presence of weak binder, HABP2, forming spherulites (Figure 3c,d). In contrast, significantly larger crystals were formed (400–800 nm in width and several μm in length), growing individually in the presence of HABP1. (Figure 3e,f).

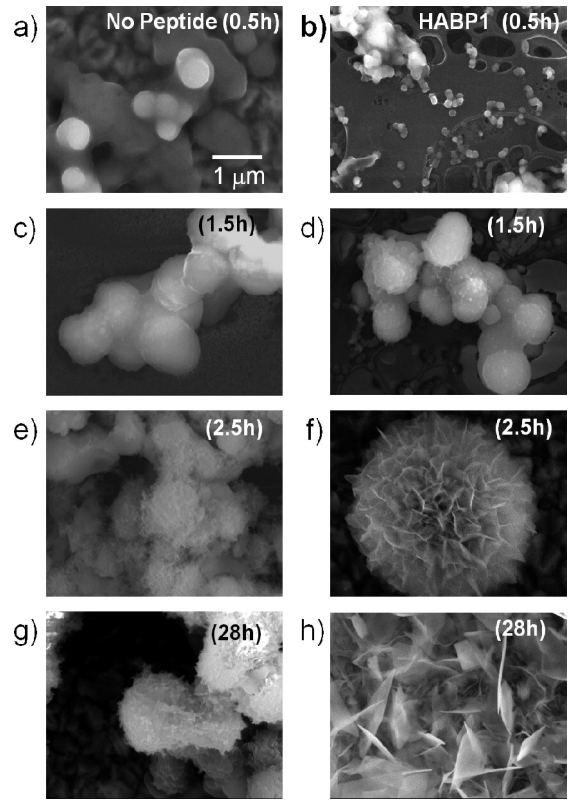

Figure 4. SEM images of minerals grown in the presence of no binder and strong binder (HABP1) at 0.5 (a,b), 1.5 (c,d), 2.5 (d,f), and 28 (g,h) hours. The scale bar in (a) applies to (b−h).

Mineralization was also monitored using SEM, which provided more detailed observation in terms of time-wise morphological evolution. At the 30 min mark, globular particles formed both in the negative control and HABP1 conditions with the dimensions of the particles formed in the latter being about 5 times smaller (100 nm) than those formed in the former (500 nm) (Figure 4a,b). Also, the number of mineral particles formed in the presence of HABP1 was significantly less than that formed in the negative control. At the 90 min mark, the size of the globular particles had grown to a similar size in both cases (~1 μm). At this time interval, whereas the particles formed in the control experimental condition were relatively smooth, those formed in the presence of HABP1 were rough, consisting of spicular features on their surfaces (Figure 4c,d). At the 2.5 h mark, the dimensions of the globular particles formed in the negative control condition did not change significantly and platelike features were still not apparent. However, in the presence of HABP1, the spicular features had been grown into platelike crystals and formed spherulites. (Figure 4e,f). Even after 28 h of reaction, there was still no significant change in the morphology of the crystals in the negative control, whereas in the presence of HABP1, the crystals attained were of significantly larger dimensions (Figure 4g,h), consistent with the TEM observations. Additional morphological changes were not observed in any of the reactions up to 96 h (data not shown). The morphological evolution of the particles formed with and without HABP1 is schematically shown in Scheme 1.

Molecular Architectural Analysis of Peptides. The observed differences in the binding affinity and effect on crystal formation of HABP1 and HABP2 suggest that there may be structural features that may potentially be attributed to the binding and mineralization activities of HA-binding peptides. To explore this issue, we performed circular dichroism (CD)

Scheme 1. Schematic Representation of Minerals Grown in the Presence of No-Binder and Strong-Binder at 0.5, 1.5, 2.5, and 28 h[a]

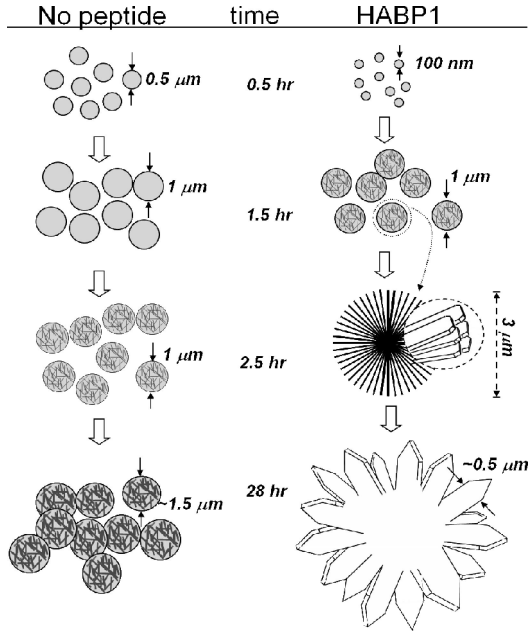

[a] Note that the particle size in the no-peptide reaction does not change even after 2.5 h of reaction while the particles grow significantly in the presence of HABP1.

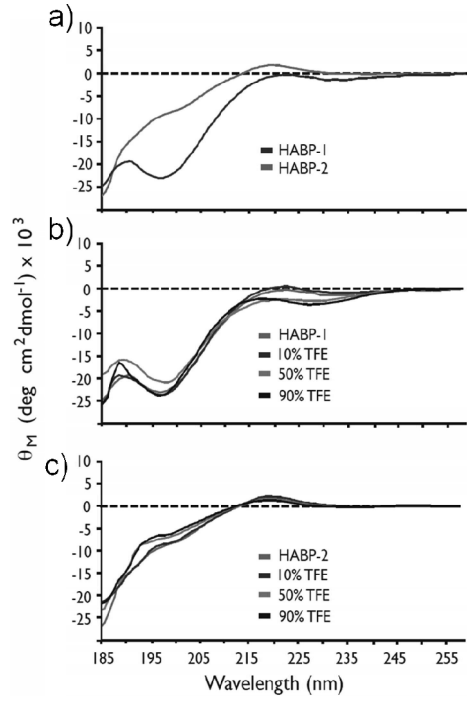

Figure 5. CD spectra of 30 μM HABP1 and HABP2 polypeptides in (a) 100 μM Tris-HCl, pH 7.5; (b,c) in the presence of varying volume percentages of TFE in 100 μM Tris-HCl, pH 7.5, respectively.

experiments on both of the synthetic peptides under identical solution conditions. As shown in Figure 5a, we observed that HABP1 and HABP2 do exhibit structural similarities but with significant conformational differences. Both sequences exhibit a (+) ellipticity band centered at 220 nm (n−π* transition). This (+) band is consistent with the presence of polyproline type II secondary structure (PPII), which has been noted in short peptides and most likely formed as a result of the presence of PPII structure-forming amino acids, Pro and Ala, in both sequences.[11] However, HABP1 possesses an additional (−) ellipticity band centered at 198 nm (π−π* transition), which is consistent with the presence of random coil or unstructured conformations.[12] Thus, HABP2 appeared to prefer the PPII conformation, whereas HABP1 existed as an equilibrium of PPII and random coil (RC) conformations. We believe that these structural differences are attributable to at least two features of the primary sequence: (a) the presence of two additional PPII forming Ala residues in the HABP2 sequence that are not found in HABP1,[11] and (b) unique potential for side chain charge repulsion between adjacent cationic His residues in HABP1, which possibly destabilizes the PPII structure of this sequence and induces RC formation.

Conformational instability is a common feature of several proteins involved in mineral formation/modification and is believed to be a driving force for polypeptide-mediated crystal growth and regulation, where interaction with mineral surfaces and/or ion clusters induces polypeptide folding or internal stabilization.[4f,12] To determine if this phenomenon exists in our HABP system, we performed additional CD experiments where the structure-stabilizing solvent, 2,2,2-trifluoroethanol (TFE), was employed (Figure 5b,c) to qualitatively evaluate the potential of these unfolded peptides to become more stable.[12a] As noted in Figure 5c, the structure of HABP2 largely persisted in the PPII conformation and was relatively unaffected by the presence of TFE up to 90% v/v. Hence, the HABP2 sequence, which has a weak effect on mineralization activity, appeared to possess a stable conformation. However, we observed that the conformation of HABP1, which had a higher binding affinity to HA and a significant effect on mineralization, did respond to the presence of TFE (Figure 5a). In particular, at TFE v/v percentages of 50% and higher, the π−π* transition band for HABP1 decreased in (+) intensity and experienced a blue-shift to 215 nm, with a minor (−) band now appearing at 225 nm. Thus, unlike HABP2, HABP1 experienced a TFE-induced conformational transition that led to the loss of PPII content as this polypeptide sequence adopted other secondary structure(s). Hence, we conclude that HABP1, and not HABP2, exhibited a greater degree of conformational instability, and this instability may be one feature that explains why this sequence is more effective at limiting crystal growth in vitro.

Mechanism of Mineralization. We note that neither peptide possesses putative Ca(II) interaction sites such as Asp or Glu; therefore, it is not directly evident how either peptide influences calcium phosphate nucleation and/or morphology. At this point, we speculate that there may be at least two plausible peptide-mediated mineralization mechanisms. The first might involve the binding of phosphate anions to the HABPs, which in turn regulate the release of phosphate anions for mineral formation. For example, the observed reduction in the mineral formation rate may be due to noncovalent interactions between HABPs and PO_4^{3-} ions, possibly via the His residues in HABP1 (hydrogen-bonding or ionic interactions) or the N, Q residues (hydrogen bonding interactions) in HABP2. If this occurred, then as PO_4^{3-} is slowly released by AP, interactions between HABPs and free PO_4^{3-} would limit the solution access of PO_4^{3-} to the active growth sites on the newly formed nuclei, which in turn would result in a slower, controlled crystal growth. At the same time, the slower kinetics may promote the formation of larger crystals instead of rapid formation of many smaller nuclei. Additional experiments with lower concentration of PO_4^{3-} as the limiting reagent would confirm this possibility, and these experiments are currently in progress. A second plausible mechanism is the direct or indirect interaction of HABPs with

newly formed mineral phase(s). Several studies have shown that the morphogenesis of biominerals can be controlled by transforming amorphous mineral precursors into crystalline phases.[1a,10b,13] Our TEM and SEM observations and Ca/P ratio measurements revealed that HABP1 accelerates the conversion of ACP to OCP. This conversion may involve interactions of HABP1 with the amorphous mineral surface, which in turn stabilizes crystal structure by lowering the surface energy, therefore resulting in a growth-dominated mineralization pathway. This mechanism of crystal maturation is also supported by our observations that similar mineral morphologies were formed in the presence of weak binder and in the negative control where no peptide was present.

The way HABPs interacts with either the ions in the solution or the crystallographic surfaces of the mineral phase may be linked to structural features that we have uncovered in our study. We find that both HABP sequences feature a common molecular thread, namely, the presence of PPII conformation, a secondary structure that features an open, extended helical conformation that allows side chain accessibility with the environment and is associated with protein intermolecular interaction processes.[11] However, the HABP1 sequence, which demonstrates a high affinity to HA and more significant control over OCP formation and morphology, also possesses some degree of disordered or RC structure and exhibits a greater degree of conformational instability. We note that conformational instability is also a feature of other native biomineralization sequences, and it has been suggested that the lack of internal structural stability somehow acts as a driving force for polypeptide interaction with ionic clusters and/or mineral surfaces.[12] Thus, HABP1 actually possesses two structural features that may enhance its ability to regulate mineralization: an extended structure that permits side chain interactions with the environment and an inherent structural instability that facilitates either polypeptide−solute or polypeptide−mineral interactions. Obviously, there may be other molecular features that contribute to this enhanced activity, another subject of future studies

Conclusion

We successfully generated a phage−peptide library for HA particles and identified a large number of clones (56) that exhibit different binding affinities to HA. Within this library, we found that two peptides with different binding affinity to HA, HABP1 (high affinity) and HABP2 (low affinity), exhibited different influences on the formation of the mineral phase in vitro. Specifically, significantly (order of magnitude) larger crystals were formed in the presence of HABP1 in comparison to those formed in the presence of HABP2 or the negative control. Although the exact mechanism of HABP-mediated mineral formation is not known, our molecular structural studies using CD show that HABP1 and HABP2 exhibit important differences with regard to primary sequence, secondary structure, and conformational stabilities. We believe that these molecular features have an impact on the observed differences in HA-binding affinities and mineralization behaviors and could be further "tweaked" to select or synthesize crystalline minerals with desired properties. The ability to control the size and the morphology of medically relevant inorganic crystals using peptides may find great use in tissue engineering applications for restoration and regeneration of the hard tissues such as bone, cartilage, and teeth.[14]Furthermore, an understanding of the structure−function relationships of small, synthetic peptides would not only offer design ideas for novel functional biomimetic materials (under the ambient conditions of aqueous solutions, room temperature and pressure, and pH about 7.0) but would also offer a deeper insight into the distinct characteristics of natural biomineralization proteins. In summary, we believe that rigorous studies, along the lines we show in this work, using other genetically selected or designed HA-binding peptides will generate a series of carefully characterized molecular regulators with which calcium phosphate mineralization could be tailored as desired, a potential novel protocol in fundamental studies in biomineralization and practical applications in tissue regeneration.

Acknowledgment. This work was supported by grants from the National Science Foundation through the Genetically Engineered Materials Science & Engineering Center (GEMSEC), and MRSEC, the U.S. Army Research Office through the Defense University Research Initiative on NanoTechnology (DURINT) program, and the Turkish State Planning Organization via Advanced Technologies in Engineering (CT). Portions of this work represent contribution no. 37 from the Laboratory of Chemical Physics, New York University (JSE).

Supporting Information Available. Additional experimental procedures and discussion on peptide selection characterization and in vitro mineralization are provided. This material is available free of charge via the Internet at http://pubs.acs.org.

References and Notes

(1) (a) Lowenstam, H. A. *Science* **1981**, *211*, 1126–1131. (b) Mann, S. In *Biomimetic Materials Chemistry*; Wiley-VCH: New York, 1996. (c) Sarikaya. M; Aksay, I. A. In *AIP Series in Polymers and Complex Materials* AIP Press: Woodbury, NY, 1995.

(2) Addadi, L.; Weiner, S. *Proc. Natl. Acad. Sci. U.S.A.* **1985**, *82*, 4110–4114.

(3) (a) Muller, W. E.; Krasko, A.; Le Pennec, G.; Schroder, H. C. *Microsc. Res. Tech.* **2003**, *62*, 368–377. (b) Albeck, S.; Addadi, I.; Weiner, S. *Connect. Tissue Res.* **1996**, *35*, 365–370. (c) Ajikumar, P. K.; Vivekanandan, S.; Lakshminarayanan, R.; Jois, S. D.; Kini, R. M.; Valiyaveettil, S. *Angew. Chem., Int. Ed.* **2005**, *44*, 5476–5479. (d) Sugawara, A.; Nishimura, T.; Yamamoto, Y.; Inoue, H.; Nagasawa, H.; Kato, T. *Angew. Chem., Int. Ed.* **2006**, *45*, 2876–2879. (e) Belcher, A. M.; Wu, X. H.; Christensen, R. J.; Hansma, P. K.; Stucky, G. D.; Morse, D. E. *Nature* **2006**, *381*, 56–58. (f) Levi, Y.; Albeck, S.; Brack, A.; Weiner, S.; Addadi, L. *Chem.—Eur. J.* **1998**, *4*, 389–396. (g) Gajjeraman, S.; Narayanan, K.; Hao, J.; Qin, C.; George, A. *J. Biol. Chem.* **2007**, *282*, 1193–1204.

(4) (a) Iijima, M; Moriwaki, Y.; Takagi, T.; Moradian-Oldak, J. *J. Cryst. Growth* **2001**, *222*, 615–626. (b) He, G.; Dahl, T.; Veis, A.; George, A. *Nat. Mater.* **2003**, *2*, 552–558. (c) Beniash, E.; Simmer, J. P; Margolis, H. C. *J. Struct. Biol.* **2005**, *149*, 182–190. (d) Sugawara, A.; Nishimura, T.; Yamamoto, Y.; Inoue, H.; Nagasawa, H.; Kato, T. *Angew. Chem., Int. Ed.* **2006**, *45*, 2876−2879. (e) Curnow, P.; Bessette, P. H.; Kisailus, D.; Murr, M. M.; Daugherty, P. S.; Morse, D. E. *J. Am. Chem. Soc.* **2005**, *127*, 15749–15755. (f) Collino, S.; Kim, I. W.; Evans, J. S. *Cryst. Growth Des.* **2006**, *6*, 839–842. (g) Prozorov, T.; Mallapragada, S. K.; Narasimhan, B.; Wang, L.; Palo, P.; Hamilton, M. N.; Williams, T. J.; Bazylinski, D. A; Prozorov, R.; Canfield, P. C. *Adv. Funct. Mater.* **2007**, *17*, 951–957. (h) Iijima, M.; Du, C.; Abbott, C.; Doi, Y.; Oldak-Moradian, J. *Eur. J. Oral Sci.* **2006**, *114*, 304–307.

(5) (a) Hartgerink, J. D.; Beniash, E.; Stupp, S. I. *Science* **2001**, *294*, 1684–1688. (b) Elhadj, S.; Salter, E. A.; Wierzbicki, A.; De Yoreo, J. J.; Han, N.; Dove, P. M. *Cryst. Growth Des.* **2006**, *6*, 197–201. (c) Shiba, K.; Honma, T.; Minamisawa, T.; Nishiguchi, K.; Noda, T. *EMBO Rep.* **2003**, *4*, 148–153.

(6) Sarikaya, M.; Tamerler, C.; Jen, A. K. Y.; Schulten, K.; Baneyx, F. *Nat. Mater.* **2003**, *2*, 577–585.

(7) (a) Brown, S.; Sarikaya, M.; Johnson, E. *J. Mol. Biol.* **2000**, *299*, 725–735. (b) Dai, H. X.; Choe, W. S.; Thai, C. K.; Sarikaya, M.; Traxler, B. A.; Baneyx, F; Schwartz, D. T. *J. Am. Chem. Soc.* **2005**, *127*, 15637–15643. (c) Dickerson, M. B.; Naik, R. R.; Stone, M. O.; Cai, Y.; Sandhage, K. H. *Chem. Commun.* **2004**, 1776–1777. (d) Gaskin, D. J. H.; Starck, K.; Vulfson, E. N. *Biotechnol. Lett.* **2000**, *22*, 1211–

1216. (e) Klem, M. T.; Willits, D.; Solis, D. J.; Belcher, A. M.; Young, M.; Douglas, T. *Adv. Funct. Mater.* **2005**, *15*, 1489–1494. (f) Naik, R. R.; Brott, L. L.; Clarson, S. J.; Stone, M. O. *J. Nanosci. Nanotechnol.* **2002**, *2*, 95–100.

(8) (a) Smith, G. P. *Science* **1985**, *228*, 1315–1370. (b) Lee, S. Y.; Choi, J. H.; Xu, Z. H. *Trends Biotechnol.* **2003**, *21*, 45–52.

(9) (a) Golub, E. E.; Harrison, G.; Taylor, A. G.; Camper, S.; Shapiro, I. M. *Bone Miner.* **1992**, *17*, 273–278. (b) Bellows, C. G.; Aubin, J. E; Heersche, J. N. M. *Bone Miner.* **1991**, *14*, 27–40. (c) Hamade, E.; Azzar, G.; Radisson, J.; Buchet, R.; Roux, B. *Eur. J. Biochem.* **2003**, *270*, 2082–2090.

(10) (a) Bodier-Houlle, P.; Steuer, P.; Voegel, J. C.; Cuisinier, F. J. *Acta Crystallogr., Sect. D: Biol. Crystallogr.* **1998**, *54*, 1377–1381. (b) Eanes, E. D.; Gillessen, I. H.; Posner, A. S. *Nature* **1965**, *208*, 365–367. (c) Legeros, R. Z.; Daculsi, G.; Orly, I.; Abergas, T.; Torres, W. *Scanning Microsc.* **1989**, *3*, 129–138. (d) Tung, M. S.; Brown, W. E. *Calcif. Tissue Int.* **1985**, *37*, 329–331. (e) Habibovic, P.; van der Valk, C. M.; van Blitterswijk, C. A.; de Groot, K.; Meijer, G. *J. Mater. Sci.: Mater. Med.* **2004**, *15*, 373–380. (f) Kamakura, S.; Sasano, Y.; Shimizu, T.; Hatori, K.; Suzuki, O.; Kagayama, M.; Motegi, K. *J. Biomed. Mater. Res.* **2002**, *59*, 29–34.

(11) (a) Chellgren, B. W.; Creamer, T. P. *Biochemistry* **2004**, *43*, 5864–5869. (b) Cubellis, M. V.; Caillez, F.; Blundell, T. L.; Lovell, S. C. *Proteins: Struct., Funct., Bioinformatics* **2005**, *58*, 880–892.

(12) (a) Kulp, J. L.; Minamisawa, T.; Shiba, K.; Evans, J. S. *Langmuir* **2007**, *23*, 3857–3863. (b) Evans, J. S. *Curr. Opin. Colloid Interface Sci.* **2003**, *8*, 48–54. (c) Seker, U. O. S.; Wilson, B; Dincer, I. S.; Kim, I. W.; Oren, E. E.; Evans, J. S.; Tamerler, C.; Sarikaya, M. *Langmuir* **2007**, *23*, 7895–7900.

(13) (a) Beniash, E.; Aizenberg, J.; Addadi, L.; Weiner, S. *Proc. R. Soc. London, Ser. B* **1997**, *264*, 461–465. (b) Volkmer, D.; Harms, M.; Gower, L.; Ziegler, A. *Angew. Chem., Int. Ed.* **2005**, *44*, 639–644.

(14) Chou, Y. F.; Huang, W. B.; Dunn, J. C. Y.; Miller, T. A.; Wu, B. M. *Biomaterials* **2005**, *26*, 285–295.

BM701037X